INVESTIGATION OF THE POTENTIAL FOR OPTIMIZATION OF HYDRAULIC AXIAL THRUST BALANCING METHODS IN A CENTRIFUGAL PUMP

D. Lefor - J. Kowalski - T. Herbers - R. Mailach*

Ruhr-Universität Bochum, Chair of Thermal Turbomachinery, 44801, Bochum, Germany,
dominik.lefor@rub.de

*Klaus Union GmbH & Co KG, 44795, Bochum, Germany

ABSTRACT

To reduce bearing loads in centrifugal pumps hydraulic axial thrust balancing methods are commonly used. Their disadvantage is the causing of significant flow losses, which result in a decline of the pump's efficiency. Within this investigation the balancing methods casing ribs and J-Grooves are compared. The objective is to determine the potential for improvement of J-Grooves concerning the pump efficiency in contrast to previously examined casing ribs. The study is carried out on the basis of a CFD model of an industrial magnetic drive pump, which is validated by transient local static pressure measurements at different operating points.
The geometry of the J-Grooves is parameterized. A stochastically based sensitivity analysis is performed, whereby the importance and correlations of the parameters are evaluated. An automatic optimization is subsequently carried out and leads to an efficiency improvement of up to 1.14 percentage points for a J-Groove design.

NOMENCLATURE

COV	var.	covariance			
F_{Shroud}	N	axial force on shroud	n	min^{-1}	rotational speed
H	m	delivery head	p	Pa	static pressure
Q	m^3/s	volume flow	η_{i}	-	internal efficiency
Q_{Opt}	m^3/s	volume flow at design point	μ	var.	expectancy value
V	var.	variance	σ	var.	standard deviation
c_{r}	m/s	radial velocity component	ϕ	°	rotation angle
c_{u}	m/s	circumferential velocity component	$n_{\mathrm{q}} = \frac{n \cdot \sqrt{Q}}{H^{0,75}}$		specific speed

INTRODUCTION

Axial thrust is a frequent problem in centrifugal pumps. Especially wet runner pumps can only hold small axial forces because of the usually applied plain bearings. For single-stage machines the only solution is the use of hydraulic axial thrust balancing methods, some of which are focused in this paper. By reason of the significant flow losses caused by these methods the objective is their optimization, whereby the internal efficiency of the pump should be improved.

For this purpose a CFD model of an industrial magnetic drive centrifugal pump is used. The default balancing methods of the pump are balancing holes and casing ribs. The seven balancing holes of the default design are retained during the optimization investigations because they cause minimal losses while they reduce the axial force component on the hub back side markedly (Guelich, 2004). This happens by pressure equalization between impeller inlet and a part of the back side

chamber, which is encapsulated by a wear ring. Hence, the focused balancing methods are used in addition to the balancing holes for further axial thrust reduction.

The goal of a previous study (Lefor et al., 2014) was the optimization of the default casing ribs, which work as eight around the circumference uniformly distributed radial swirl breaking vanes at the casing wall inside the front side chamber. The reduced swirl decreases the radial pressure gradient inside the chamber, with the result that the high pressure at the impeller outlet can spread out into the chamber and the axial force component on the shroud wall of the side chamber increases and works against the resulting force, which is orientated towards the suction side. The chaotic flow conditions in the front side chamber, which originate from the swirl breaking and secondary flow (Guelich, 2004), made a specific optimization most difficult. Therefore, a stochastically based method has been chosen. At first on basis of geometrically parameterized casing ribs a sensitivity analysis has been performed to identify important and unimportant parameters. Afterwards an EA-optimization has been carried out with the influential parameters. The major characteristics of the computed best design are a number of 14 ribs and a very large thickness so that the space between the ribs gets very small. This leads to a geometry which has no more ribs, but grooves in a closer arranged casing wall instead. So called J-Grooves, which are radial grooves in the casing wall, are introduced by Kurokawa et al. (1994) and Abe et al. (2006). In comparison to casing ribs they break the swirl in the side chamber as well and have a specific influence on the secondary flow additionally. This effect is illustrated in figure 1. Because of centrifugal forces a radial outward flow occurs at the impeller wall and as a consequence of the continuity condition inside the front side chamber a radial inward flow occurs at the casing wall. Inside the J-Grooves no circumferential velocity component is possible, whereby the inward flow is channeled and the radial velocity rises. Because of the continuity condition the radial outward velocity at the impeller wall rises, too, and the circumferential component decreases. Thus, rotation and radial pressure gradient decrease, the counteracting force on the impeller shroud increases and reduces the resulting axial force.

Since the recent investigations have indicated grooves as a good alternative to casing ribs, the objective of this work is to find an optimal J-Groove design. Because of the chaotic flow conditions in the front side chamber, the J-Grooves are designed and optimized by means of stochastic procedures.

CFD MODEL

The current investigations of this paper are based on the same pump model as the mentioned previous work (Lefor et al., 2014). Machine data and CFD configuration are given in tables 1 and 2. The model has been generated with Ansys ICEM and Ansys CFX. Steady state as well as transient computations have been carried out for different operating points. Previously, the model quality has been proved and a validation has been conducted by means of the characteristic curve, axial thrust measurement and transient local static pressure measurement. A section view of the numerical hexahedral mesh is given in figure 2 and shows the division into five domains and the interpolating interfaces in between. Furthermore the used balancing methods balancing holes and casing ribs of the industrial pump's default design are marked.

A supplement to the validation measurement follows next. In the experiment the transient static pressure is recorded at seven measuring points, which are depicted in figure 3. S1, S2 and S3 are placed in the casing wall of the front side chamber, S6 in the rear side chamber, S5 and S7 in the volute and S4 in the suction port. The experiment is performed with the default design pump but without casing ribs. In addition to the operating point $Q/Q_{\mathrm{Opt}} = 0.95$ a part load ($Q/Q_{\mathrm{Opt}} = 0.74$) and an overload ($Q/Q_{\mathrm{Opt}} = 1.13$) operating point are considered. The results of the measurement and the corresponding transient CFD computation are plotted over one impeller rotation in figures 3 a-c. The measured pressure signals are averaged over 200 impeller rotations. The corresponding standard deviation is shown in the chart. For more details of the experimental setup the authors refer to the

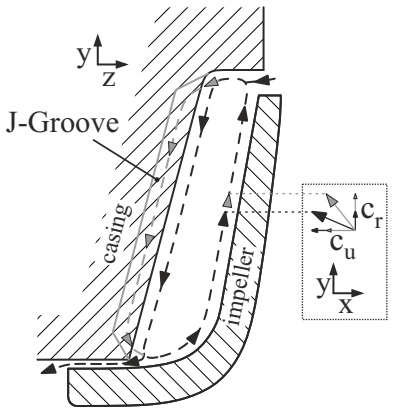

Figure 1: **Influence of J-Groove on secondary flow**

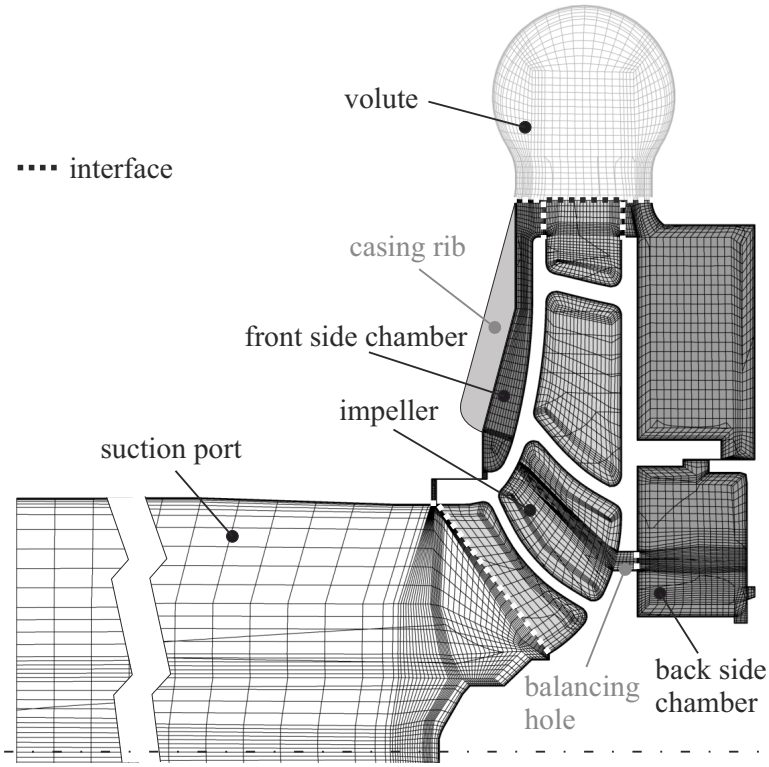

Figure 2: **Section view of the computational mesh with domains**

Rotational speed	1480 RPM
Specific speed	24.1
Impeller diameter	405 mm
Number of blades	7
Delivery head	50 m

Table 1: **Machine data**

Parameter	**Description**
Medium	Water at 20 $°C$
Turbulence model	SST
Inlet boundary	Mass flow
Outlet boundary	Ave. static pressure
Transient time step	0.362 ms $\widehat{=}\ \Delta\phi = 3.21\,°$
Element number	2797552
Mesh wall distance	0.05 mm

Table 2: **CFD configuration**

recent work (Lefor et al., 2014).

For all signals a repeating behavior with a periodic time of one blade passing can be observed. An excellent qualitative accordance of experiment and CFD can be stated in all points except S4, which has nearly a constant value in the CFD results because of the input boundary condition of constant mass flow. For some measurement points offsets can be observed. S3, S6 and S7 values have a good coincidence at part load, a small deviation at $Q/Q_{\mathrm{Opt}} = 0.95$ and a maximum offset at overload, which is of 2.6 % for S3. An increasing deviation between CFD and experimental results with a rising flow rate has already been noted for the characteristic curve in the recent work (Lefor et al., 2014). Limbach et al. (2014) observed the same effect with higher deviations for a centrifugal pump with low specific speed of 12 and volute casing. Due to the simultaneous increase of deviation and

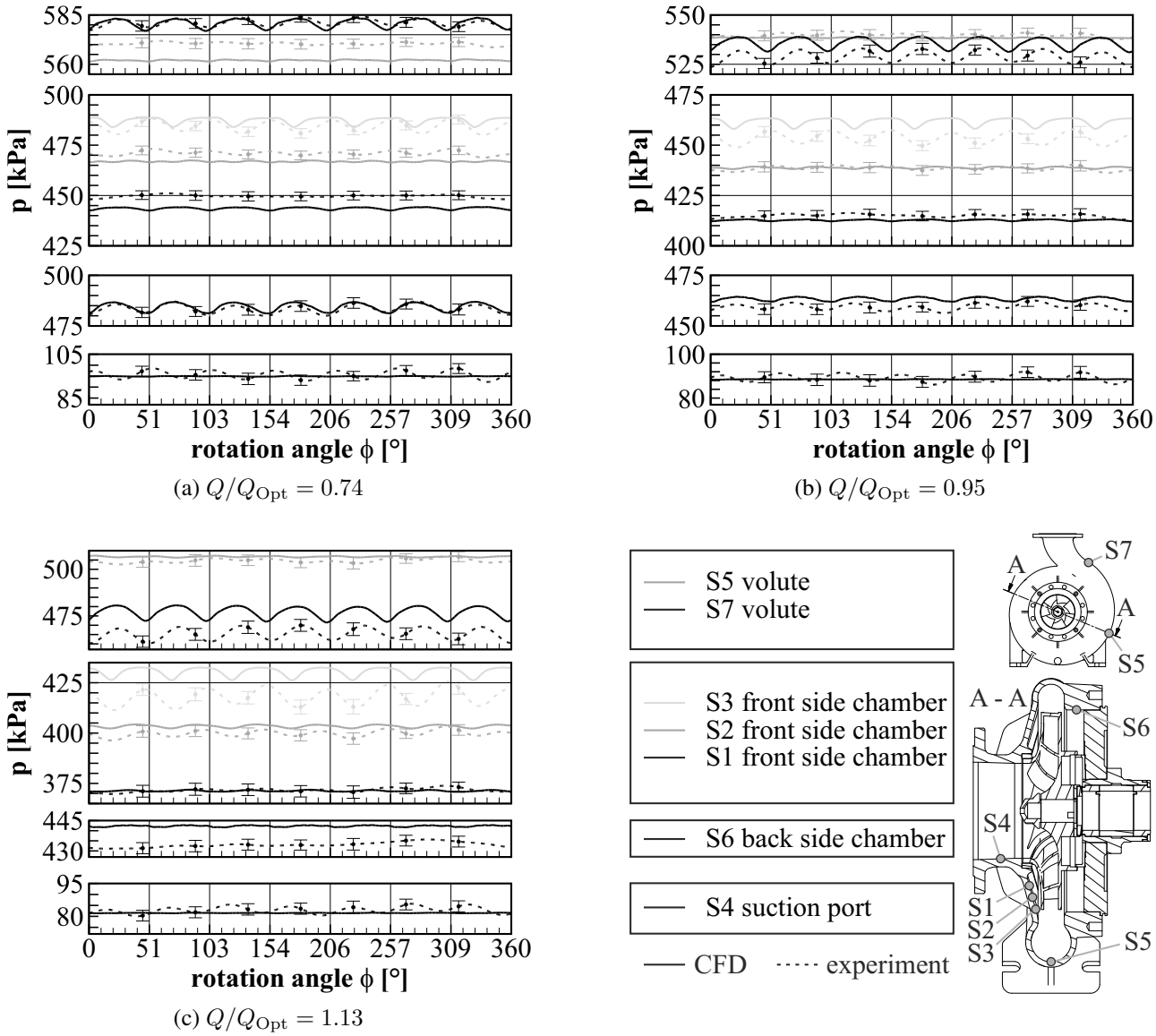

(a) $Q/Q_{\mathrm{Opt}} = 0.74$

(b) $Q/Q_{\mathrm{Opt}} = 0.95$

(c) $Q/Q_{\mathrm{Opt}} = 1.13$

Figure 3: **Results of local transient static pressure measurement**

flow velocity in machines with large surfaces, it can be assumed that friction effects are insufficiently reproduced in the CFD. The resulting losses might be to small and lead to a higher pressure at the pressure side of the pump in the CFD computation than it is measured in the experiment (S3, S6, S7). However, for the examined pump with a medium specific speed of 24.1 adequate flow prediction with minor deviations can be achieved.

APPROACH AND SETUP OF THE OPTIMIZATION

In the impeller side chamber a rotational core flow with half rotor angular velocity exists between stationary casing wall and rotating impeller wall (Wesche, 2012). Additionally, the above-mentioned radial secondary flow superposes. If furthermore rotationally periodic installed balancing methods disturb the rotationally symmetric flow, the effects of specific geometry changes in the framework of an optimization are hard to estimate. For that reason a stochastically based optimization method is used.

The approach is schematically shown in figure 4. At first a model is generated with Ansys Work-

bench. Instead of the default casing ribs geometrically parameterized J-Grooves are added to the CAD geometry of the front side chamber domain, whereby multiple designs are possible. Next the geometry of the current design is automatically meshed with tetrahedral elements and prism layers at the walls, which is conform to the hexahedral configuration. The domain is then integrated into the CFD model of the whole pump for which some simplifications are applied to reduce the calculation time. The computation is performed in steady state with frozen rotor interfaces and a coarser mesh resolution with a scaling factor of 0.125 for the number of elements is used for the remaining domains. The calculation time for one design amounts to 12 hours on a system with 12 Intel Xeon X5660 cores. After the calculation the internal efficiency and axial force components are given out as responses by the postprocessor.

Next up a sensitivity analysis is carried out with the software Dynardo Optislang. A random sampling of designs is performed with advanced latin hypercube sampling (ALHS) by use of the before introduced Workbench model. By means of correlation coefficients meaningful and unimportant geometric parameters can be identified (Most and Will, 2011). Moreover, a regression model called MOP (Metamodel of Optimal Prognosis) is automatically created by Optislang and can be used for further correlation analysis (Most and Will, 2010).

In the framework of the following optimization an objective has to be defined at first, which is the optimal internal efficiency. Additionally, a constraint is defined to ensure the required axial force reduction. Furthermore, a best possible start design is taken from the sampling, the MOP or a preoptimization. In order to finally iterate a best design, various algorithms, such as gradient based methods, adaptive response surface method (ARSM) or evolutionary algorithm (EA) are available in Optislang (Dynardo, 2013). The required designs can be calculated on the model or taken from the MOP if its prediction quality is sufficient, which is often not the case for CFD investigations, such as in the studies of Cremanns et al. (2013), Einzinger (2013) or Lefor et al. (2014).

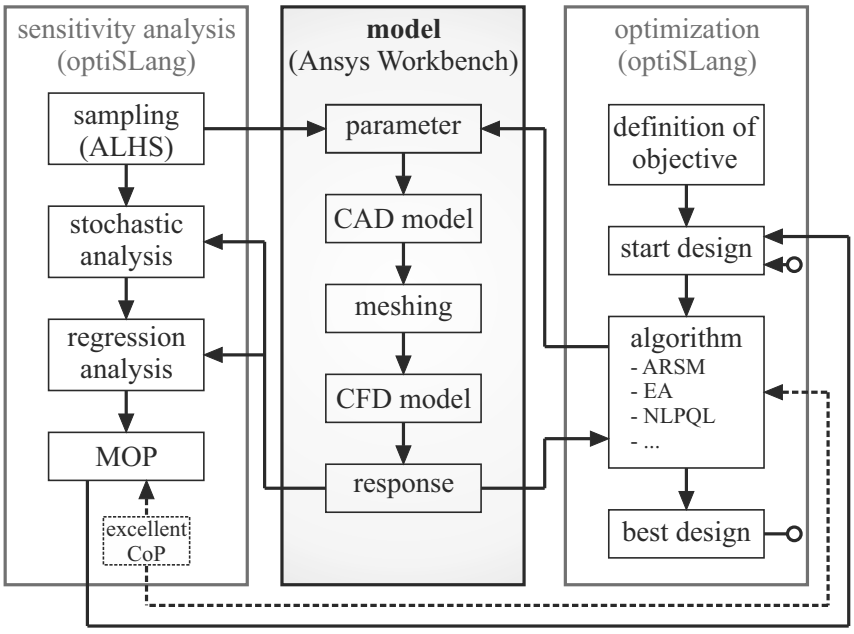

Figure 4: **Scheme of the optimization approach (Lefor et al., 2014)**

IMPROVEMENT BY USE OF J-GROOVES

The results of the recent work (Lefor et al., 2014) suggest that J-Grooves might be an improvement compared to casing ribs in respect of the pump efficiency. The goal is to find a low-loss design,

which achieves the same axial force reduction as the casing ribs. In order to find a suitable version, a parameterized J-Groove geometry is created for the front side chamber domain. With the before outlined approach it is possible to find an optimum design with a constraint for a non changing axial force component on the shroud. Since no start design exists, the sensitivity analysis is used to find one, which fulfils this constraint.

Geometrical Parameterization

The parameterization of the J-Grooves is shown in figure 5. The parameters p_gap and p_gap2 allow the reduction of the distance between casing wall and impeller at two points. Since the casing ribs of the default design are closer to the impeller wall than the J-Grooves, these parameters allow to obtain a similar strength of influence (compare figure 2 and 5). Without these parameters the intended axial force reduction might be impossible. The parameter p_h controls the depth and p_lgth the length of the grooves, whereby the outer start radius is fixed. Furthermore the width is regulated by p_width. The number of J-Grooves around the circumference is determined by p_numb. This parameterization allows the creation of nearly any conceivable design. A curvature of the groove has been excluded because a corresponding parameter has been detected as unimportant in the recent casing rib investigation. Besides it disagrees with the previously explained functional principle of the J-Groove. The ranges for the parameters and the manually chosen start design are given in table 3. For p_lgth relative values are used.

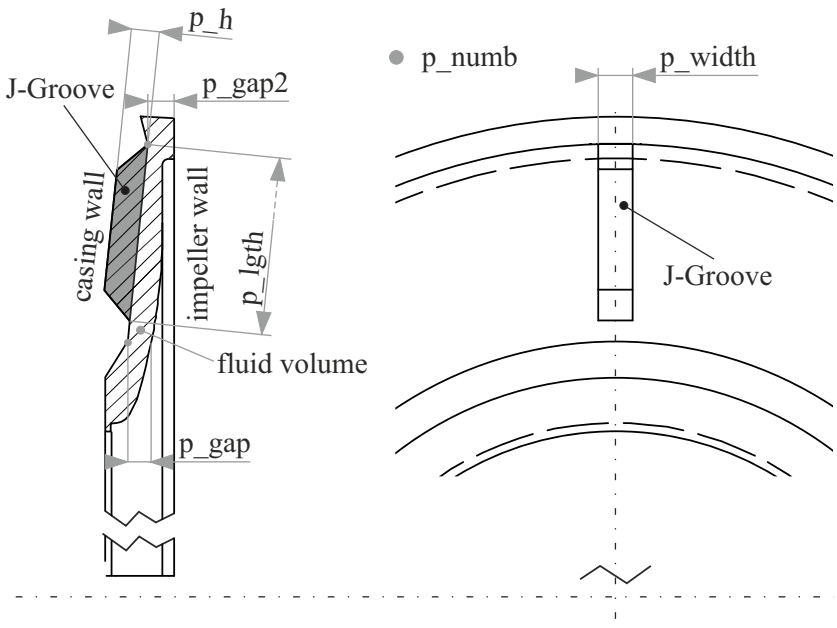

Figure 5: **Parameterized geometry of J-Groove**

Sensitivity Analysis

The Workbench model with the embedded parameterized front side chamber domain is initially used to create a sampling of 127 random designs with ALHS. The responses of the simulation, which are the internal efficiency η_{i} and the axial force component on the shroud F_{Shroud}, are used to identify influential and unimportant parameters. Furthermore, the MOP regression model is created.

For the investigation of the correlation of the parameters and the responses the coefficient of correlation, which is defined in equation 1, is used. It is the covariance of two variables X and Y normalized by the product of their standard deviations (Kohn and Öztürk, 2010). Consequently it

represents the linear correlation. A coefficient of correlation of zero means no correlation whereas a value of one is the maximum correlation. Negative values state a opposite behavior (Most and Will, 2011).

$$\rho(X,Y) = \frac{COV(X,Y)}{\sigma_X \sigma_Y} \tag{1}$$

Figure 6 shows the corresponding correlation matrix for each two parameters or responses. On the upper left side the coefficients of correlation are shown and on the lower right side the different designs are depicted as points. The strongest influence on η_i and F_Shroud can be stated for p_numb. With a larger number of grooves the axial force component on the shroud, which is negatively orientated and counteracts the resulting axial force, decreases (increase of its magnitude), but the internal efficiency decreases as well with a similarly strong impact. So this parameter is useful to roughly adapt the demanded axial force reduction, but not to improve the efficiency. A similar behavior can be observed for p_width with less influence. The enlargement of any parameter value cannot obtain an efficiency improvement, because all the parameters extend the flow resistance in the front side chamber. The goal is to find a design with the least necessary flow impact to achieve the best possible efficiency. Parameter p_h has the third largest impact on the responses, whereby the correlation coefficient with η_i is lower than with F_Shroud. This parameter may be used for a fine adjustment. The correlations of the other parameters with the responses are markedly lower. The length of the J-Groove p_lgth has a small variation range and starts on maximum radius. A length shorter than 70 % of maximum is not possible to generate because of the chamfers at both ends which are included in the length value (see figure 5). However, a shorter J-Groove should not be aspired because the channelling effect would rapidly decrease. Balancing methods are most effective on high radius where higher pressure is present. The correlation coefficients of p_gap and p_gap2 are small, but they might still have potential to raise the value of F_Shroud by decreasing the distance to the impeller. For p_gap the efficiency is negatively affected, whereas p_gap2 has almost no influcence on η_i.

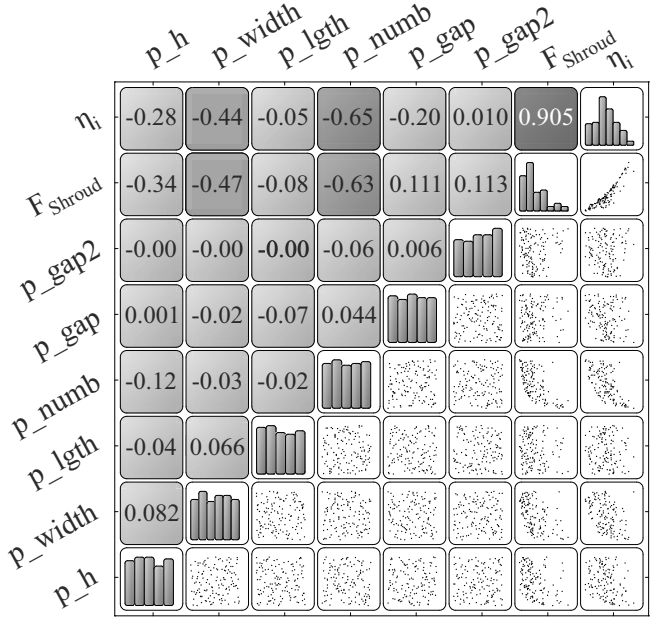

Figure 6: **Coefficients of correlation matrix**

Parameter	Min	Max
p_numb	2	40
p_gap	4 mm	24.77 mm
p_gap2	7 mm	13.7 mm
p_h	0.75 mm	20 mm
p_lgth	0.7	1
p_width	2 mm	20 mm

Table 3: **Parameter variation**

Furthermore for η_i and F_Shroud some regression models are calculated by Optislang. The Meta-models of Optimal Prognosis (MOP), which are those with the best prediction quality, are given in

table 4. A quadratic polynomial regression (QPR) has been chosen for η_{i} and a moving least square method (Lancaster and Salkauskas, 1980) for F_{Shroud}. Some variables are filtered because they have minor or even negative influence on the regression models (Dynardo, 2013). The prediction quality has been evaluated with the Coefficient of Prognosis (CoP) (Most, T., Will, J., 2008, 2011):

$$CoP = 1 - \frac{\sum_{i=1}^{N}(y_i - \hat{y}_i)^2}{\sum_{i=1}^{N}(y_i - \mu_Y)^2} \tag{2}$$

The residual variance of a variable Y, in which $\hat{y}_i$ is the approximation value, is normalized with the variance of Y. The CoP differs from the common Coefficient of Determination by the definition of the residual variance. For Y values from the sampling are picked here which have not been used to build up the regression model. The CoP values are ranged between 0 and 1. The CoPs for η_{i} and F_{Shroud} can be taken from table 4. The model for the axial force component has a very good prediction quality. A value of 0.9 for the efficiency is reasonable for CFD models in general, but however too small to forecast the small improvements this investigation is about. Hence, the MOP is inapplicable for the later optimization.

A further correlation index to ascertain the importance of the geometric parameters is the CoP for single variables. It is defined as the product of the global CoP and the total effect sensitivity index:

$$CoP(X_j) = CoP \cdot \left(1 - \frac{V(Y|X_{\sim j})}{V(Y)}\right) \tag{3}$$

The total effect sensitivity index includes the variance of Y and the variance of Y without the examined input parameter X_j. The CoPs for the geometric parameters are shown in table 4 as well. Just as for the coefficients of correlation the parameters p_numb and p_width have the largest impact on both output variables. A lower influence can be stated for p_numb, too. For the models of both outputs the variables p_lgth and p_gap2 and for the model of F_{Shroud} also p_gap have already been left out for the regression model. So their influence is even smaller. In contrast to the before mentioned correlation coefficients the $CoP(X_j)$ detects a larger influence on η_{i} for all parameters.

The manually chosen best design for the J-Groove (JG sens.) is listed in table 5. Its efficiency improvement is 0.83 percentage points in contrast to the default casing rib design of the optimization model (OM), but the axial force component on the shroud is slightly below the requirement. Nevertheless, the design is suited as start design for the following optimization.

Optimization

For the optimization an adaptive response surface method (ARSM) has been chosen and carried out with Dynardo Optislang. It is recommended for CFD optimizations because it needs less solver runs than other methods and smooths solver noise (Dynardo, 2013). The functional principle is schematically presented in figure 7. The algorithm starts on the best design from the sensitivity analysis. Based on support points around the current best design (BD) an approximated response surface is created by a DOE scheme using linear polynomial. If existing, a new best design is selected upon this surface an validated by a solver run. A local moving and shrinking function modifies the considered space from iteration to iteration (Dynardo, 2013). The parameters p_lgth and p_gap2, which have been filtered in the MOPs of both models, are kept constant with the values from the sensitivity analysis best design.

The iterated best design (JG ARSM), which results from 13 iteration steps with 78 design calculations, is given in table 5. The internal efficiency has been improved by 0.82 percentage points and the axial force on the shroud has approximately remained constant referring to the optimization model with the default design. The characteristic features of the design are a large number of J-Grooves and

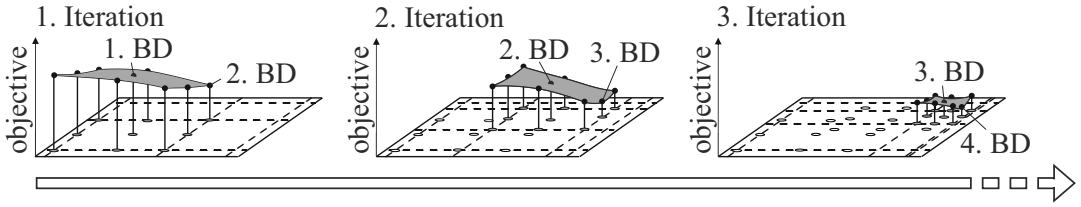

Figure 7: **Scheme of ARSM-optimization (Dynardo, 2013; Stander and Graig, 2002)**

a small gap between the casing and the impeller wall. The values for the parameters p_h and p_width are in the middle range.

	η_{i}	F_{Shroud}
model	QPR	MLS
CoP	0.90	0.97
$\mathrm{CoP}_{\mathrm{p\_numb}}$	0.47	0.55
$\mathrm{CoP}_{\mathrm{p\_gap}}$	0.07	filtered
$\mathrm{CoP}_{\mathrm{p\_gap2}}$	filtered	filtered
$\mathrm{CoP}_{\mathrm{p\_h}}$	0.15	0.18
$\mathrm{CoP}_{\mathrm{p\_lgth}}$	filtered	filtered
$\mathrm{CoP}_{\mathrm{p\_width}}$	0.21	0.24

Table 4: **Coefficients of Prognosis**

Param.	**Default (OM)**	**CR EA**	**JG sens.**	**JG ARSM**
p_numb	-	-	37	40
p_gap	-	-	4.73 mm	7.21 mm
p_gap2	-	-	8.57 mm	8.57 mm
p_h	-	-	14.90 mm	12.43 mm
p_lgth	-	-	0.76	0.76
p_width	-	-	11.99 mm	14.23 mm
η_{i}	80.10 %	80.60 %	80.93 %	80.92 %
F_{Shroud}	-46097 N	-46099 N	-46015 N	-46098 N

Table 5: **Parameters and responses during optimization**

Because of the model simplifications of the optimization the best J-Groove design has been recalculated with the hexa-meshed transient configuration. The results show an even larger improvement of 1.14 percentage points between default casing rib design and the best design.

Analysis of Best Design

A closer look at the front side chamber flow is necessary to understand how and why the optimized designs work. As can been seen in figure 8 a-c, two cylindrical analysis surfaces, which extend into axial direction, are created on the radii 170 mm and 195 mm for the default casing rib design, the optimized casing rib design and the optimized J-Groove design. Figures 8 d-f show the circumferential fluid velocity component on rolled out sections of these surfaces. Behind the casing ribs wake spaces can be ascertained, which effect a reduction of the fluid rotation in the whole chamber whereby the radial pressure gradient decreases and the axial force component on the shroud increases. This leads to a lower resulting axial force. The J-Grooves, shown in figure f, reduce the rotation in the chamber as well.

The difference between casing ribs and J-Grooves can be explained by means of the radial velocity component, which is shown in figures 8 g-i. Radial inward flow with $c_{\mathrm{r}} < 0$ can be observed in a wide area of the default design. Between the optimized large and high casing ribs in figure 8 h cavities are formed which partly channel the radial inward flow, but the number of cavities is too small to catch the entire inward mass flow. The J-Groove design features a sufficient number of cavities with a constant profile in radial direction so that all the radial inward flow is channeled. The front side chamber flow is thereby less disturbed and the losses decrease. Furthermore, the radial outward velocity at the

impeller wall increases and reduces the rotational component whereby the counteracting axial force on the shroud increases as well. These effects have initially been supposed and described based on the results of the previous optimization of the casing ribs.

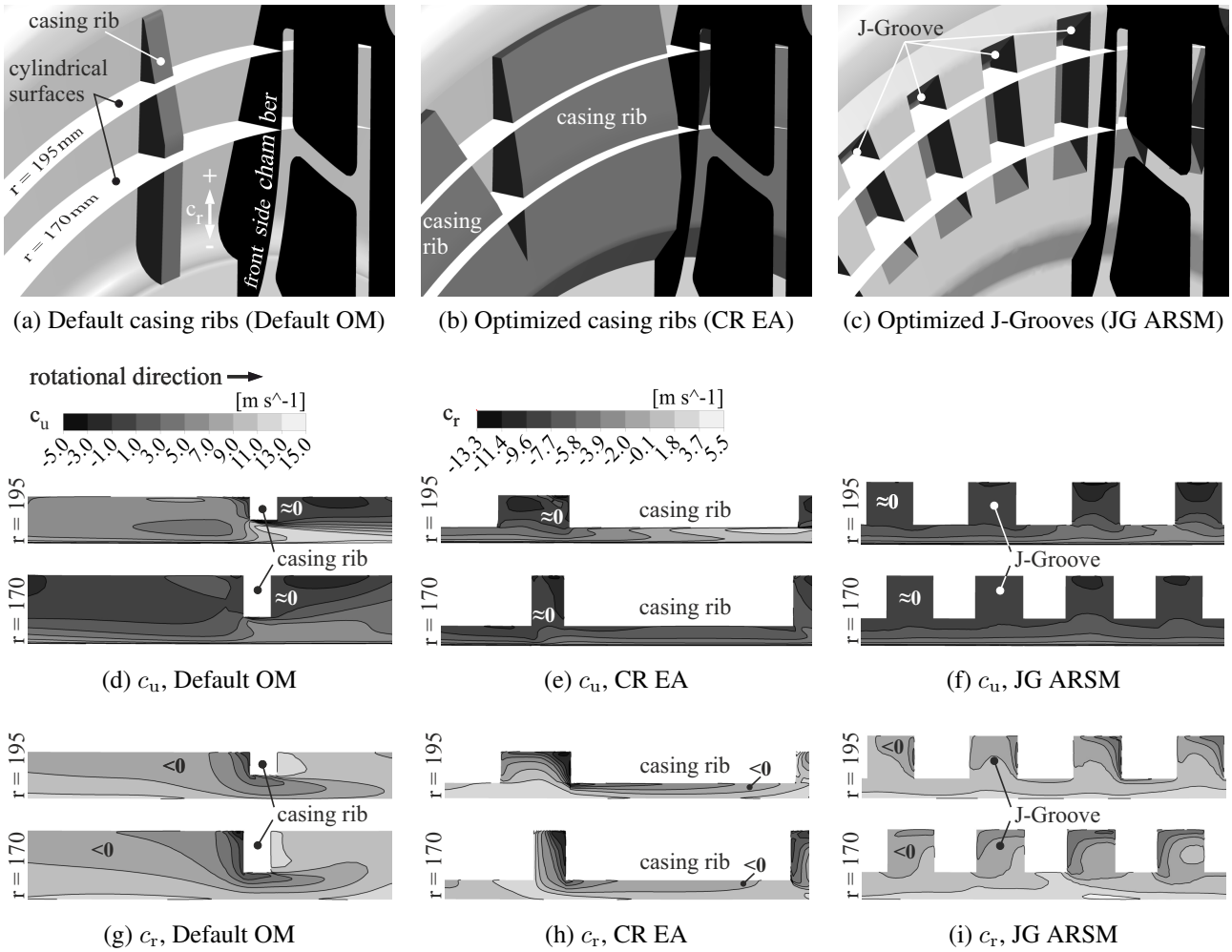

(a) Default casing ribs (Default OM) (b) Optimized casing ribs (CR EA) (c) Optimized J-Grooves (JG ARSM)

(d) c_u, Default OM (e) c_u, CR EA (f) c_u, JG ARSM

(g) c_r, Default OM (h) c_r, CR EA (i) c_r, JG ARSM

Figure 8: **Radial and circumferential velocity components on a section of the rolled out cylindrical surfaces in front side chamber on basis of the optimization models OM**

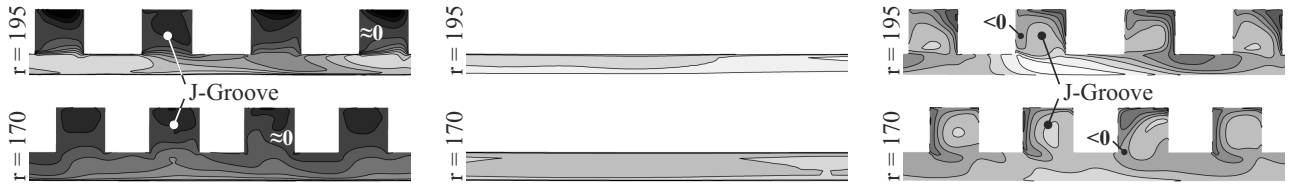

(a) c_u, JG ARSM-transient (b) c_u, JG ARSM-transient with removed grooves (c) c_r, JG ARSM-transient

Figure 9: **Radial and circumferential velocity components on a section of the rolled out cylindrical surfaces in front side chamber on basis of transient models**

Figure 9 shows velocity components for the transient models of the best J-Groove design and a design in which the J-Grooves are removed but the parameters p_gap and p_gap2 accord with the best

J-Groove design. A comparison of figures a and b illustrates the before mentioned decrease of the fluid rotation using J-Grooves, which effects the axial thrust reduction. As can be seen from figure c, the channeling of the radial inward flow within the grooves can be observed in the transient model, too. In comparison with the steady state model (figure 8 i) the grooves can not take the entire inward flow. However, some regions of high outward flow occur near the impeller wall and compensate this disadvantage.

CONCLUSIONS

In this paper the optimization potential of axial thrust balancing methods in the front side chamber of an industrial centrifugal pump has been studied on basis of previous investigations (Lefor et al., 2014). The prior optimization of casing ribs has indicated that radial grooves in the casing wall of the front side chamber may be an efficient alternative to the ribs because they channel most of the radial inward flow of the secondary flow whereby the front side chamber flow becomes more consistent. These assumption has been confirmed with the help of a parameterized radial J-Groove geometry, which has been used within a stochastic sensitivity analysis and optimization method. This approach has been suitable because the effects of geometry changes on the chaotic front side chamber flow are hard to predict. Furthermore, it has been a requirement to achieve the same axial thrust reduction as the default design with the casing ribs. Hence, the optimization method has not only been used to iterate a best design, but also to find a suitable design for the axial force constraint. The internal efficiency has been improved by 1.14 percentage points compared to the default design.

In further investigations the side chamber flow will be examined in more detail to understand the functional principle of the grooves more precisely. Moreover, the design of the back side chamber with the application of back pump-out vanes will be studied. It shall be analyzed if they come into question as an alternative to the balancing methods in the front side chamber.

ACKNOWLEDGEMENTS

The development work was conducted as a part of the research program ”Kompetenzzentrum Hydraulische Strömungsmaschinen” (Competence Center for Hydraulic Machinery) at the Ruhr-Universität Bochum, which is supported by the Ministerium für Wirtschaft, Energie, Industrie, Mittelstand und Handwerk des Landes NRW (Ministry of Economic Affairs, North Rhine-Westphalia, Germany). The authors gratefully acknowledge Klaus Union GmbH Co. KG for their support and permission to publish this paper. The responsibility for the content lies solely with its authors.

REFERENCES

Abe, H., Matsumoto, K., Kurokawa, J., Matsui, J., Choi, Y.-D. (2006), *Analysis and Control of Axial Thrust in Centrifugal Pump by Use of J-Groove*, 23rd IAHR Symposium - Yokohama.

Cremanns, K., Roos, D., Grassmann, A. (2013), *Conventional partwise optimization vs. multidisciplinary optimization of the last stage of a low pressure steam turbine with an axial radial diffuser*, Proceedings of the 10th Weimar Optimization and Stochastic Days, Weimar, Germany.

Dynardo (2013), *Methods for Multi-Disciplinary Optimization and Robustness Analysis*, Dynardo GmbH, Weimar, Germany.

Einzinger, J. (2013), *Design and Optimization of Turbo Charger Turbine Maps by Meta-Model of optimal Prognosis*, lecture, Proceedings of the 10th Weimar Optimization and Stochastic Days, Weimar, Germany.

Gülich, J. F. (2004), *Kreiselpumpen*, 2., Berlin, Heidelberg, New York, Springer.

Kohn, W., Öztürk, R. (2010), *Statisktik für Ökonomen*, Heidelberg, Dordrecht, London, New York, Springer.

Kurokawa, J., Kamijo, K., Shimura, T. (1994), *Axial Thrust Behavior in LOX-Pump of Rocket Engine*, Journal of Propulsion and Power, Vol. 10, Number 2, pp. 244-250.

Lancaster, P., Salkauskas, K. (1980), *Surface Generated by Moving Least Squares Methods*, Mathematics of Computation 155, pp. 141-158.

Lefor, D., Kowalski, J., Kutschelis, B., Herbers, T., Mailach, R. (2014), *Optimization of Axial Thrust Balancing Swirl Breakers in a Centrifugal Pump Using Stochastic Methods*, Proceedings of the ASME 2014 4th Joint US-European Fluids Engineering Division Summer Meeting, Chicago, USA.

Limbach, P., Kimoto, M., Deimel, C., Skoda, R. (2014), *Numerical 3D Simulation of the Cavitating Flow in a Centrifugal Pump With Low Specific Speed and Evaluation of the Suction Head*, Proceedings of the ASME 59th Turbo Expo, Düsseldorf, Germany.

Most, T., Will, J. (2008), *Metamodel of Optimal Prognosis - An automatic approach for variable reduction and optimal meta-model selection*, Proceedings of the Weimar Optimization and Stochastic Days 5.0, Weimar, Germany.

Most, T., Will, J. (2010), *Recent advances in Metamodel of Optimal Prognosis*, Proceedings of the Weimar Optimization and Stochastic Days 7.0, Weimar, Germany.

Most, T., Will, J. (2011), *Sensitivity analysis using the Metamodel of Optimal Prognosis*, Proceedings of the Weimar Optimization and Stochastic Days 8.0, Weimar, Germany.

Stander, N., Graig, K. (2002), *On the Robustness of a Simple Domain Reduction Scheme for Simulation-Based Optimization*, Engineering Computations 19, pp. 431-450.

Wesche, W. (2012), *Radiale Kreiselpumpen*, Heidelberg, Dordrecht, London, New York, Springer.